ACS APPLIED MATERIALS & INTERFACES

Research Article

Cite This: ACS Appl. Mater. Interfaces 2017, 9, 35642-35650

www.acsami.org

Active Antioxidizing Particles for On-Demand Pressure-Driven Molecular Release

Yongbeom Seo,[†] Jiayu Leong,[†,‡] Jye Yng Teo,[†,‡] Jennifer W. Mitchell,[§] Martha U. Gillette,[∥] Bumsoo Han,[⊥] Jonghwi Lee,[#] and Hyunjoon Kong*[,†,▽]

[†]Department of Chemical and Biomolecular Engineering, University of Illinois at Urbana−Champaign, Urbana, Illinois 61801, United States

[‡]Institute of Bioengineering and Nanotechnology, 31 Biopolis Way, The Nanos, Singapore 138669, Singapore

[§]Department of Cell and Developmental Biology, Neuroscience Program, Beckman Institute for Advanced Science & Technology, University of Illinois at Urbana−Champaign, Urbana, Illinois 61801, United States

[∥]Department of Cell and Developmental Biology, Department of Bioengineering, Neuroscience Program, Beckman Institute for Advanced Science & Technology, University of Illinois at Urbana−Champaign, Urbana, Illinois 61801, United States

[⊥]School of Mechanical Engineering, Birck Nanotechnology Center, Purdue Center for Cancer Research, Purdue University, 585 Purdue Mall, West Lafayette, Indiana 47907, United States

[#]Department of Chemical Engineering and Materials Science, Chung-Ang University, Seoul 156-756, South Korea

[▽]Department of Chemical and Biomolecular Engineering, Department of Bioengineering, Institute for Genomic Biology, University of Illinois at Urbana−Champaign, Urbana, Illinois 61801, United States

Supporting Information

ABSTRACT: Overproduced reactive oxygen species (ROS) are closely related to various health problems including inflammation, infection, and cancer. Abnormally high ROS levels can cause serious oxidative damage to biomolecules, cells, and tissues. A series of nano- or microsized particles has been developed to reduce the oxidative stress level by delivering antioxidant drugs. However, most systems are often plagued by slow molecular discharge, driven by diffusion. Herein, this study demonstrates the polymeric particles whose internal pressure can increase upon exposure to H_2O_2, one of the ROS, and in turn, discharge antioxidants actively. The on-demand pressurized particles are assembled by simultaneously encapsulating water-dispersible manganese oxide (MnO_2) nanosheets and green tea derived epigallocatechin gallate (EGCG) molecules into a poly(lactic-*co*-glycolic acid) (PLGA) spherical shell. In the presence of H_2O_2, the MnO_2 nanosheets in the PLGA particle generate oxygen gas by decomposing H_2O_2 and increase the internal pressure. The pressurized PLGA particles release antioxidative EGCG actively and, in turn, protect vascular and brain tissues from oxidative damage more effectively than the particles without MnO_2 nanosheets. This H_2O_2 responsive, self-pressurizing particle system would be useful to deliver a wide array of molecular cargos in response to the oxidation level.

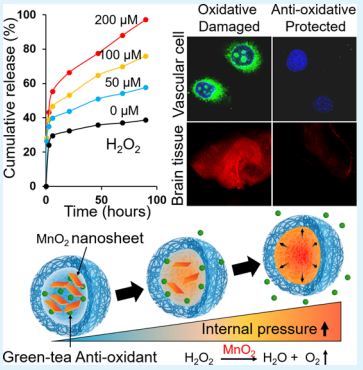

KEYWORDS: *oxidative damage, hydrogen peroxide (H_2O_2), MnO_2 nanosheets, poly(lactic-co-glycolic acid) (PLGA) particle, epigallocatechin gallate (EGCG)*

1. INTRODUCTION

Reactive oxygen species (ROS) such as superoxide anion and H_2O_2 play a major role in various physiological processes, including cell signaling, proliferation, differentiation, and immune response.[1−3] However, abnormal overproduction of ROS increases the oxidative stress level of living cells and subsequently stimulates cell death.[4−7] Such undesirable oxidative damage is often associated with inflammation, ischemia, infection, stroke, traumatic brain injury, diabetes mellitus, and cancer.[7−14]

In recent years, extensive efforts were made to prevent the ROS-induced increase of intracellular oxidative stress by administering various types of antioxidative drugs.[15−18] These antioxidants were often encapsulated in nano- or microsized biodegradable polymeric particles to sustain an antioxidizing effect.[17−20] It is desirable that particles release the antioxidative drug cargos continuously, at a constant rate in response to an increase of the ROS level. However, most particle systems are plagued by the slow molecular release over time. Subsequently, the controllable range of molecular release rate is very narrow, and a significant fraction of antioxidants remains in the particles during the desired treatment period.[21−23]

Received: August 16, 2017
Accepted: September 29, 2017
Published: September 29, 2017

ACS Publications © 2017 American Chemical Society

DOI: 10.1021/acsami.7b12297
ACS Appl. Mater. Interfaces 2017, 9, 35642−35650

Herein, this study presents an active antioxidizing polymeric particle that can self-pressurize and, in turn, release a controlled amount of antioxidative drug molecules actively in response to an increase of the ROS level. These particles serve to protect living cells and tissues from oxidative damage. We hypothesized that polymeric particle designed to generate oxygen (O_2) gas through the chemical reaction with H_2O_2 would discharge the antioxidants actively in an oxidative environment because of the increased internal pressure of the particle. The subsequent increase in released antioxidants would be advantageous to prevent ROS-induced cell death and tissue degeneration.

The hypothesis was examined by loading water-dispersible MnO_2 nanosheets complexed with alginate into PLGA particles together with drug molecules (Scheme 1). The MnO_2 nanosheets would generate O_2 gas by decomposing H_2O_2 and increase the internal pressure of the particles. In addition, MnO_2 can decompose H_2O_2 without generating highly reactive hydroxyl radicals and dissociates into biologically inert Mn^{2+} ions.[24,25] The H_2O_2-responsive molecular release kinetics of PLGA particles was analyzed by loading bovine serum albumin molecules as model molecular cargos under varying H_2O_2 concentration. The PLGA particles were also loaded with antioxidative EGCG molecules to evaluate their capability to protect endothelial cells and brain tissues from H_2O_2-induced oxidative damage.

Scheme 1. Schematic Illustration of the Assembly of the PLAG Particles Enabling on-Demand, Pressurized Molecular Release[a]

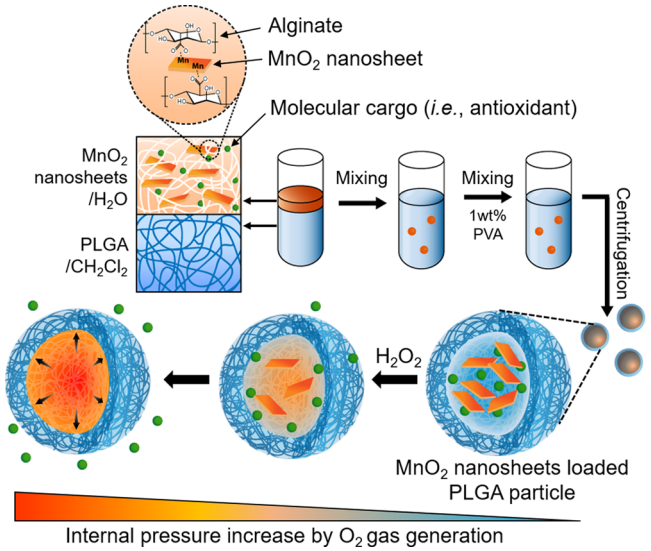

[a]The water-dispersible MnO_2 nanosheets and antioxidant molecules are loaded into PLGA particle through double emulsion method. The resulting MnO_2 nanosheet-loaded PLGA particle can increase the internal pressure by generating O_2 gas via reaction with H_2O_2. In turn, the particle can discharge antioxidants actively and improve efficacy to protect cells and tissues from oxidative damage.

2. EXPERIMENTAL SECTION

2.1. Materials. Alginate (MW ≈ 250000 g mol^{-1}) was obtained from FMC Biopolymer. Cellulose filter was purchased from Millipore Inc. 2-(*N*-morpholino)ethanesulfonic acid (MES), potassium permanganate ($KMnO_4$), bovine serum albumin (BSA), poly(vinyl alcohol) (PVA, MW = 9000−10000), epigallocatechin gallate (EGCG), fluorescein amine, 1-hydroxybenzotriazole hydrate, rhodamine B isothiocyanate (RBITC), and L-glutamine were purchased from Sigma-Aldrich. PLGA (lactic:glycolic = 50:50, MW = 6000−10000 g mol^{-1}) was purchased from LACTEL. H_2O_2 (30% solution) was purchased from Macron Fine Chemicals. 1-Ethyl-3-(dimethylaminopropyl)carbodiimide hydrochloride, Pierce BCA Protein Assay Kit, Pierce Quantitative Peroxide Assay Kit, CellROX Green, propidium iodide, and Penicillin-Streptomycin were purchased from Thermo Scientific.

2.2. Synthesis of Water-Dispersible MnO_2 Nanosheets and Alginate-Free MnO_2 Sheets. Alginate was dissolved in distilled water at a concentration of 1.0% (w/v). The alginate solution was filtered with a 0.22 μm cellulose filter and freeze-dried. Filtered alginate was dissolved in 0.1 M MES buffer solution (pH 6) at a concentration of 2.0% (w/v). Water-dispersible MnO_2 nanosheets were prepared by adding 500 μL of 50 mM $KMnO_4$ into 500 μL of alginate solution and then sonicating the solution for 30 min. In the case of alginate-free MnO_2 sheets, MES buffer without alginate was used instead of the alginate solution.

2.3. Assembly of PLGA Micro- And Nanoparticles Loaded with Bovine Serum Albumin (BSA) and MnO_2 Nanosheets. PLGA micro- and nanoparticles loading BSA and MnO_2 nanosheets were prepared via a double emulsification (W_1/O/W_2). Water phase 1 (W_1) was prepared by adding 10 mg of BSA to a 1.0 mL MnO_2 nanosheets dispersion. 200 μL of the mixture solution (W_1) was then added to the organic phase (O), and 750 μL of dichloromethane dissolved with 10 mg of PLGA. The mixture was vortexed to prepare microparticles. Or, the mixture was sonicated to prepare nanoparticles. Both vortex mixing and sonication were conducted for 5 min to form the W_1/O emulsion. This primary emulsion (W_1/O) was then transferred to 6 mL of 1 wt % aqueous PVA solution (W_2). Then, the mixture was vortexed or sonicated again for 5 min to form the secondary emulsion (W_1/O/W_2). The mixture was continuously stirred uncapped for 6 h. The resulting microparticles and nanoparticles were collected by centrifugation at 2000 and 12000 rpm for 10 min, respectively, and washed with cell culture-grade water. This purification process was repeated three times.

2.4. Assembly of PLGA Microparticles Encapsulated with EGCG and MnO_2 Nanosheets. PLGA microparticles loaded with EGCG and MnO_2 nanosheets were prepared by a similar method described above. Water phase 1 (W_1) was prepared by adding 1.0 mg of EGCG in 1.2 mL of the MnO_2 nanosheets dispersion. 400 μL of the mixture solution (W_1) was then added to the organic phase (O), 1.5 mL of dichloromethane dissolved with 20 mg of PLGA. The mixture was vortexed to prepare microparticles for 5 min. This primary emulsion (W_1/O) was then transferred to 6 mL of 1 wt % aqueous poly(vinyl alcohol) solution (W_2). Then, the mixture was vortexed or sonicated again for 5 min to form the secondary emulsion (W_1/O/W_2). The mixture was continuously stirred for 6 h while cap was off. The resulting microparticles and nanoparticles were collected by centrifugation at 2000 rpm for 10 min and washed with the cell culture-grade water. This purification process was repeated three times.

2.5. Synthesis of Fluorescently Labeled Alginate and BSA. Alginate (100 mg, 0.5 mmol COOH) dissolved in MES buffer was labeled with fluorescein amine, isomer I using aqueous carbodiimide chemistry. 1-Hydroxybenzotriazole hydrate (0.08 mmol), fluorescein amine (0.002 mmol dissolved in methanol 1 mg/mL), and 1-ethyl-3-(dimethylaminopropyl)carbodiimide hydrochloride (0.16 mmol) were added sequentially to the alginate solution. The reaction mixture was left stirring at room temperature and protected from light for 4 h. Then, the modified alginate was purified by dialysis against DI water over 2 days and finally lyophilized to a yellow, foamlike solid.

BSA (100 mg, 4 mg/mL) dissolved in the sodium carbonate/bicarbonate buffer (0.1 M, pH 9.0) was labeled with RBITC. RBITC (4 mg, dissolved in DMSO 2 mg mL^{-1}) was added dropwise to the BSA solution. The reaction mixture was left stirring at room temperature and protected from light for 4 h. Then, the modified BSA was purified by dialysis against DI water over 2 days and finally lyophilized to a pink, foamlike solid.

DOI: 10.1021/acsami.7b12297
ACS Appl. Mater. Interfaces 2017, 9, 35642−35650

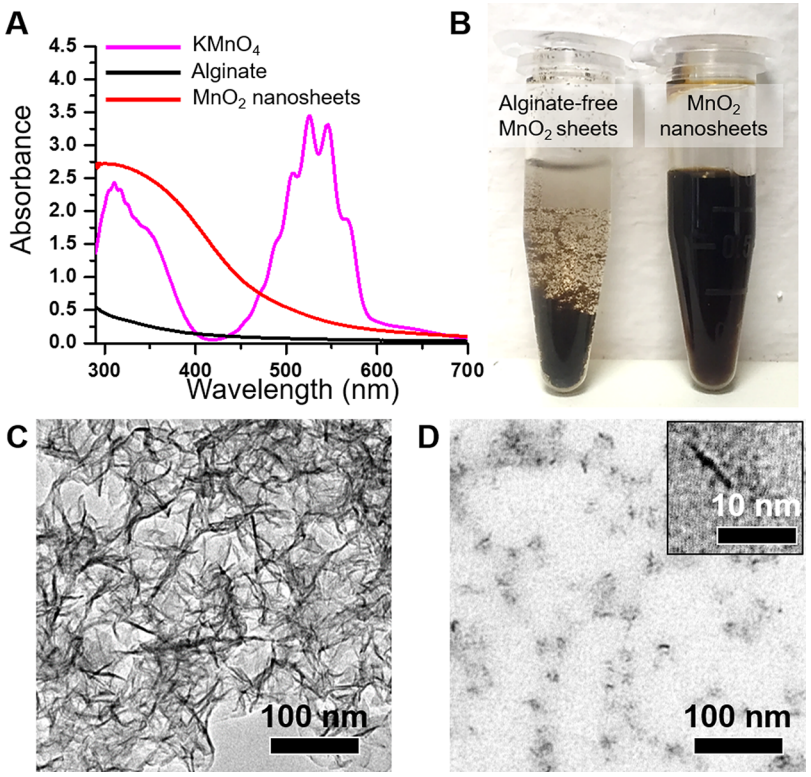

Figure 1. Water-dispersible MnO_2 nanosheets complexed with alginate. (A) UV−vis absorption spectra of $KMnO_4$, alginate, and MnO_2 nanosheets solutions. (B) Photo images of the alginate-free MnO_2 sheets and MnO_2 nanosheets suspended in the aqueous medium. (C and D) (C) TEM images of alginate-free MnO_2 sheets and (D) MnO_2 nanosheets complexed with alginate, denoted as MnO_2 nanosheets. In (D), the image in the box shows a single MnO_2 nanosheet.

2.6. Characterization of Particles. The optical and confocal microscopic images of PLGA microparticles were obtained by the optical microscope (Leica DMIL) and the confocal microscope (Carl Zeiss LSM 700), respectively. For scanning electron microscopy (SEM) imaging of microparticles, PLGA particle suspensions were frozen at −20 °C and then lyophilized. The SEM images of PLGA microparticles were obtained with HITACHI S-4800 microscope operating at 2.0 kV. For transmission electron microscopy (TEM) imaging of nanoparticles, a few droplets of solutions were placed on a TEM microgrid, which was followed by drying under ambient conditions. The TEM images of MnO_2 nanosheets and PLGA nanoparticles were obtained using JEOL 2100 TEM with an accelerating voltage of 200 kV. The elemental analysis of manganese within PLGA particles was conducted by the inductively coupled plasma atomic emission spectroscopy (ICP/AES). The size distribution and zeta potential of nanoparticles were determined in the distilled water at room temperature by using the dynamic light scattering (DLS, Malvern Zetasizer NanoZS). The size distribution of microparticles was obtained by image analysis with ImageJ software.

2.7. Analysis of the Molecular Release Profile and the Reactivity to H_2O_2. Each sample of PLGA particles was suspended in 2 mL of PBS with different H_2O_2 concentrations (i.e., 0, 50, 100, and 200 μM) and incubated at 37 °C under continuous shaking at 100 rpm. At the designated time points, PLGA particles were collected by centrifugation. Then, the concentrations of BSA and H_2O_2 of the supernatant were determined using the Pierce BCA Protein Assay Kit and Pierce Quantitative Peroxide Assay Kit according to manufacturer's instructions, respectively.

For analysis of the EGCG release from particles, PLGA particles were suspended in 10 mL of PBS with 200 μM H_2O_2 and incubated at 37 °C under continuous shaking at 100 rpm. At the designated time points, PLGA particles were collected by centrifugation. Then, the concentrations of EGCG in the supernatant were determined by reading the absorbance at wavelength of 250 nm using the microplate spectrophotometer (Infinite 200 PRO, Tecan).

2.8. Analysis of the Metabolic Activity of Endothelial Cells. Mouse endothelial cell line, C166 (ATCC CRL2581), was maintained in DMEM growth media supplemented with 10% FBS, 1 mM sodium pyruvate, 100 U/mL penicillin and 100 mg/mL streptomycin, and cultured at 37 °C, under an atmosphere of 5% CO_2 and 95% humidified air. C166 cells were seeded onto 96-well plates at a density of 8000 cells per well 1 day before treatment. By doing so, cells formed a thin endothelium. 200 μM and 400 μM H_2O_2 solutions were prepared by serial dilutions in the cell culture media without sodium pyruvate. The cells were then incubated with PLGA particles encapsulating only EGCG or those encapsulating both EGCG and MnO_2 nanosheets. Ten microliters of PLGA particles (10 mg/mL) was added to 100 μL of fresh media for 2 h at 37 °C. After 2 h, 100 μL of growth media and 10 μL of MTT solution were then added to each well. The cells were incubated for 4 h at 37 °C. The formazan crystals formed in each well were solubilized using 120 μL of DMSO upon removal of growth media. The absorbance values of MTT at wavelength of 550 and 690 nm were measured by using the microplate spectrophotometer. The relative metabolic activity of cells was quantified as $[(A_{550} - A_{690})_{sample}/(A_{550} - A_{690})_{control}]$.

2.9. Imaging Analysis of the Intracellular Oxidative Stress. C166 cells were seeded onto glass coverslips placed onto 12-well plates at a density of 100000 cells per well 1 day before treatments. 200 μM H_2O_2 solution was prepared by serial dilutions in cell culture media without sodium pyruvate. The cells were then incubated with PLGA particles encapsulating only EGCG or those encapsulating both EGCG and MnO_2 nanosheets. 100 μL of PLGA particles (10 mg/mL) was added to 1 mL of fresh media with sodium pyruvate for 2 h at 37 °C. After 1.5 h, the cells were stained for 30 min at 37 °C with 5 μM of CellROX Green to assess the intracellular oxidative stress level. After 30 min, the cells were washed with PBS and fixed with 3.7% formaldehyde for 15 min, washed with PBS, and stained with 300 nM DAPI. Then, cells were imaged by using the confocal microscopy.

2.10. Organotypic Hippocampal Brain Tissue Slice Culture. All experiments were performed in compliance with the Guide for

DOI: 10.1021/acsami.7b12297
ACS Appl. Mater. Interfaces 2017, 9, 35642−35650

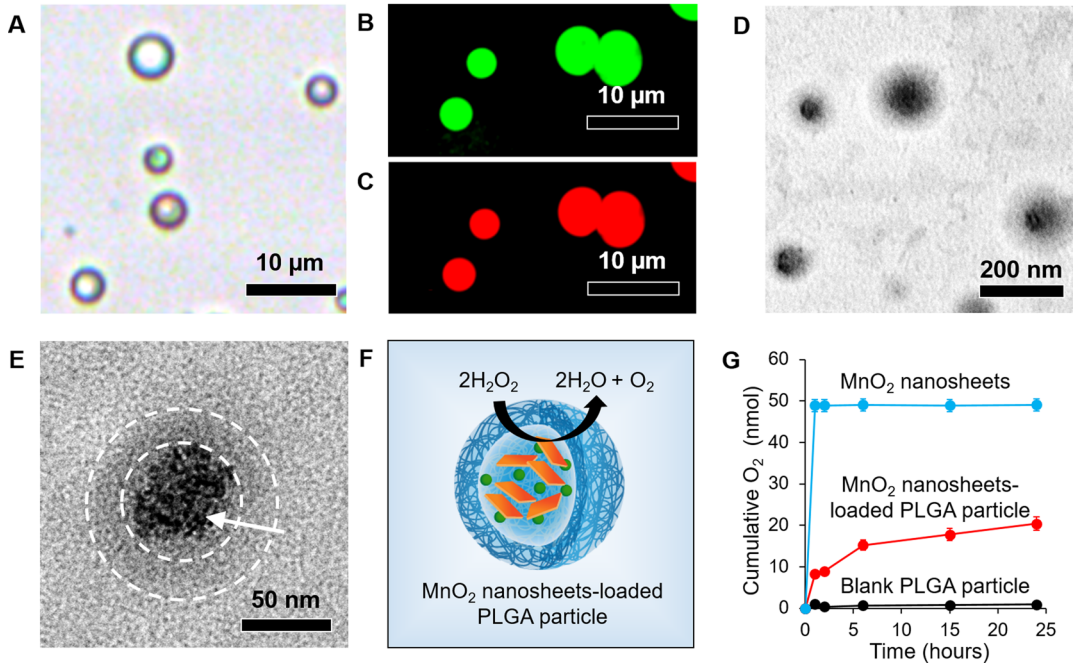

Figure 2. Morphology and O_2-generating ability of the PLGA particles loading MnO_2 nanosheets and BSA. (A) Optical microscopy image of the PLGA microspheres. (B and C) Confocal image of MnO_2 nanosheets and BSA loaded in the PLGA microspheres. Alginates complexed with MnO_2 nanosheets were labeled with green-colored fluorescein while BSA molecules were labeled with red-colored rhodamine. (D and E) TEM images of the PLGA nanospheres loaded with the MnO_2 nanosheets. In (E), the dotted line represents the PLGA shell and arrow indicates MnO_2 nanosheets localized in the core of PLGA nanospheres. (F) Scheme of the O_2 generation within MnO_2 nanosheets-loaded PLGA particles exposed to H_2O_2. (G) Measurement of cumulative O_2 amount in the media after adding blank PLGA particles, MnO_2 nanosheets-loaded PLGA particle, and free MnO_2 nanosheets.

Care and Use of Laboratory Animals of the National Institutes of Health and approved by the Institutional Animal Care and Use Committee at the University of Illinois at Urbana−Champaign (Animal Welfare Assurance A3118-01). Brains of 7 days old Long-Evans rat pups from our inbred colony (LE/BluGill) were removed and immersed in the ice-cold slicing media (93 mM *N*-Methyl-D-glucamine, 2.5 mM KCl, 1.2 mM NaH_2PO_4, 30 mM $NaHCO_3$, 20 mM HEPES, 25 mM glucose, 2 mM thiourea, 3 mM sodium pyruvate, 10 mM $MgSO_4$, 0.5 mM $CaCl_2$, pH 7.4) bubbled with CO_2. Hippocampi were isolated from 350 μm coronal brain slices sectioned by vibrotome (Leica VT1000S). Slices were transferred to tissue culture inserts (0.4 μm; Millicell-CM, Millipore) contained within 35 mm tissue culture dishes. The dishes were immersed in 1 mL of organotypic media (DMEM without sodium pyruvate supplemented with 10 mM HEPES, GS21 (1:50, GlobalStem), Penicillin-Streptomycin (1:100), and 1 mM L-glutamine. Cultures were kept at 37 °C in 5% CO_2, and media were exchanged every other day. Brain slices were kept in culture for 1 week.

2.11. Analysis of the Oxidation-Induced Brain Tissue Necrosis. For the oxidative stress test, tissue cultures were transferred to the organotypic media with 5 μM propidium iodide (7.5 mM stock in distilled water) and 200 μM H_2O_2 at 33 °C for 2 h. Control slices were not exposed to H_2O_2. To evaluate the antioxidizing activity of PLGA particles, the organotypic media was mixed with PLGA particles encapsulating only EGCG or those encapsulating both EGCG and MnO_2 nanosheets. The final PLGA particle concentration in the organotypic media was 1 mg mL^{-1}. Membranes with the brain slices were then rinsed twice in the Hank's Buffered Salt Solution (HBSS) and fixed overnight with 4% paraformaldehyde. The tissue necrosis level was assessed by fluorescence from the propidium iodide incorporated into necrotic cells. The confocal microscopy (Zeiss 510 meta) was used for imaging. 100% Cell death was defined by a maximal final propidium iodide signal obtained from slices incubated for 16 h at 4 °C in the presence of 5 μM propidium iodide. ImageJ software was utilized to determine the total tissue fluorescence (integrated density − background). Cell death was expressed as a percentage of the maximal signal.

3. RESULTS AND DISCUSSION

3.1. Synthesis and Characterization of Water-Dispersible MnO_2 Nanosheets. Water-dispersible MnO_2 nanosheets complexed with alginate, denoted as MnO_2 nanosheets, were synthesized by adding 50 mM of potassium permanganate ($KMnO_4$) solution to the 2-(*N*-morpholino)ethanesulfonic acid (MES) buffer dissolved with 2 wt % alginate. The mixture solution was sonicated for 30 min. Alginate-free MnO_2 sheets were also prepared as a control. In accordance with the UV−vis absorption spectra, the characteristic peaks of $KMnO_4$ appearing at 315, 525, and 545 nm disappeared during the reduction in MES buffer (Figure 1A). Instead, a broad absorption around 350 nm appeared, which is a characteristic of MnO_2 nanomaterials.[24] This result indicates the reduction of $KMnO_4$ by MES buffer and the formation of MnO_2 nanosheets. Due to complexation with alginate, the resulting MnO_2 nanosheets complexed with alginate remained stable in aqueous media for 30 days (Figure 1B). No precipitation was observed during this period. In contrast, the alginate-free MnO_2 sheets rapidly aggregated and precipitated within 2 h.

The morphology of MnO_2 nanosheets was characterized and compared with alginate-free MnO_2 sheets, using a high-resolution transmission electron microscopy (TEM). Alginate-free MnO_2 sheets were in the form of aggregates whose size was much larger than 1000 nm (Figure 1C and Figure S1). In contrast, MnO_2 nanosheets with alginate were in a rectangular form with 1 nm thickness and sub-10 nm length, while the shadow around MnO_2 nanosheets indicates the existence of alginate polymers (Figure 1D and Figure S1). The

DOI: 10.1021/acsami.7b12297
ACS Appl. Mater. Interfaces 2017, 9, 35642−35650

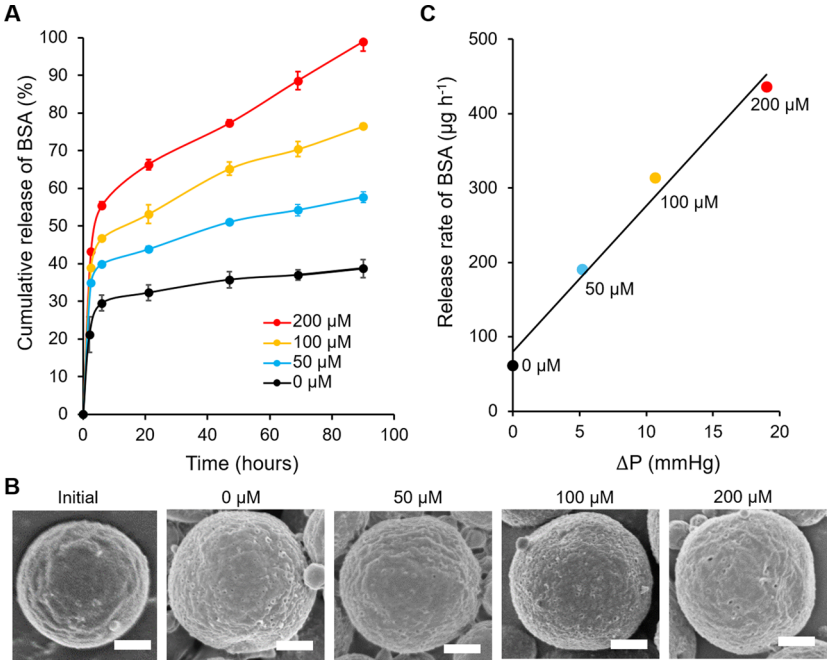

Figure 3. BSA release from PLGA microparticles loaded with MnO_2 nanosheets in oxidative environment. (A) Cumulative release profiles of BSA from PLGA microparticles loaded with MnO_2 nanosheets. Particles were incubated in the PBS with different concentrations of H_2O_2 (i.e., 0 to 200 μM). (B) SEM images of PLGA microparticles before and after incubation in PBS with different concentrations of H_2O_2 for 22 h. No visible holes or cracks were observed. The scale bar represents 1.0 μm. (C) The release rate of BSA versus the hydraulic pressure difference (ΔP) of the PLGA particle. The number noted next to each dot represents the H_2O_2 concentration in the media.

mean hydrodynamic diameter of the alginate-MnO_2 nanosheets complex was 40 nm, as determined by the dynamic light scattering (DLS) measurement (Figure S2). On the other hand, MnO_2 nanosheets showed a much lower zeta potential value (−37 mV) than alginate-free MnO_2 sheets (−17 mV) (Figure S3). This result suggests that alginate restricted the sintering and aggregation of MnO_2 nanosheets by complexing on the surface. Also, the increased electrostatic repulsion helped MnO_2 nanosheets remain stable in aqueous media.

3.2. Preparation of MnO_2 Nanosheets-Loaded PLGA Particles. The H_2O_2-responsive, self-pressurizing PLGA particles were assembled by simultaneously encapsulating MnO_2 nanosheets and BSA through the double emulsification process coupled with vortex mixing. The resulting PLGA particles showed a hollow spherical shape with a mean diameter of 4 μm (Figure 2A and Figure S4). The MnO_2 nanosheets and BSA molecules encapsulated in the core of PLGA microspheres were confirmed by using fluorescein-conjugated alginate and rhodamine B-conjugated BSA molecules (Figure 2, panels B and C). The encapsulation efficiencies for MnO_2 nanosheets and BSA molecules were 10 and 50%, respectively.

Nanosized PLGA particles could also be prepared through the double-emulsification process coupled with ultrasonication. The TEM results show that the MnO_2 nanosheets were well-encapsulated in the core of PLGA nanospheres (Figure 2 (panels D and E). On the other hand, the DLS analysis revealed that the mean hydrodynamic diameter of nanoparticles was approximately 200 nm (Figure S4).

3.3. On-Demand Pressure-Driven Molecular Release. We analyzed the ability of the MnO_2 nanosheets-loaded PLGA particles to generate O_2 gas by measuring the concentration change of H_2O_2 mixed with phosphate buffer saline (PBS, pH 7.4, 100 μM H_2O_2) at 37 °C. Since O_2 gas is generated by the decomposition of H_2O_2 in solution, the consumption of H_2O_2 is directly proportional to the amount of O_2 gas generated (Figure 2F). The addition of the PLGA particles loaded with MnO_2 nanosheets in the H_2O_2 solution resulted in a gradual increase of O_2 amount over 24 h (Figure 2G and Figure S5). In contrast, the blank PLGA particles made a negligible change in the O_2 amount. The addition of free MnO_2 nanosheets (i.e., nanosheets not encapsulated in the PLGA particles) led to the rapid initial increase (i.e., within 1 h) of O_2 amount followed by a minimal change. The results confirm that the MnO_2 nanosheets encapsulated in PLGA microparticles can decompose H_2O_2 and generate O_2 gas in a more sustained and controlled manner than the free MnO_2 nanosheets.

In parallel, the molecular release profile of the PLGA microparticle loaded with MnO_2 nanosheets was characterized by measuring the amount of BSA discharged into the PBS solution mixed with H_2O_2. In this analysis, the concentration of H_2O_2 was varied from 0 to 50, 100, and 200 μM, to encompass the physiological range of H_2O_2 level.[12,26] As shown in Figure 3A, at the first time point, BSA molecules were burst out from PLGA microparticles. The initial molecular burst was mainly caused by the BSA associated with or partially embedded in the surface layer of PLGA microparticles.[27−29] After the initial burst, all samples displayed a near-zero-order release profile of BSA but with different slopes. Interestingly, the release rate of BSA, calculated by fitting the cumulative amounts of BSA released between 6 and 90 h to a linear curve, was approximately proportional to the concentration of H_2O_2 (Figure S6). In accordance with the scanning electron microscopy images of particles, the surface of the PLGA particles presented no macro-sized pores or cracks regardless of the concentration of H_2O_2 (Figure 3B and Figure S7). This result indicates that the increment of BSA release rate was not due to the damage on the surface but to the internal pressure change of PLGA microparticles. On the other hand, MnO_2

DOI: 10.1021/acsami.7b12297
ACS Appl. Mater. Interfaces 2017, 9, 35642−35650

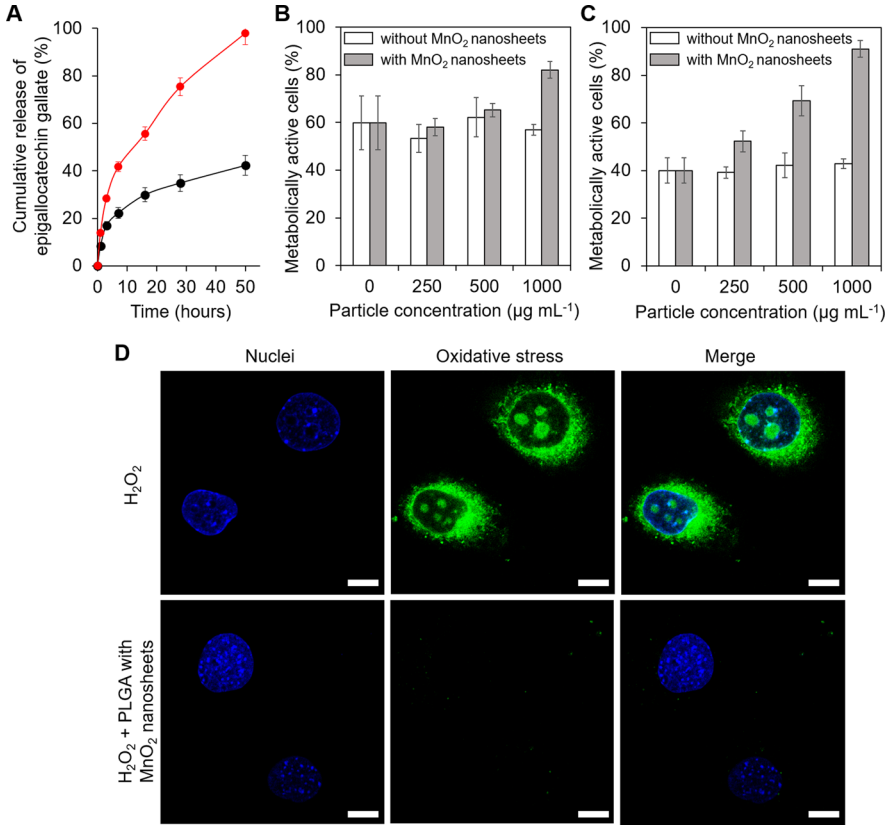

Figure 4. Activity of PLGA microparticles to protect endothelial cells from oxidative damage. (A) Cumulative release profiles of EGCG from PLGA microparticles loaded with (red) and without (black) MnO_2 nanosheets. Particles were incubated in the PBS with 200 μM H_2O_2. (B and C) MTT assay-based quantification of the metabolically active C166 endothelial cells after incubation in the media containing (B) 200 μM H_2O_2 and (C) 400 μM H_2O_2. The varying concentrations of PLGA particles were incubated on the endothelial cells cultured at confluence. The open and filled bars represent the particles without and with MnO_2 nanosheets, respectively. (D) Representative confocal images of oxidative stress of endothelial cells incubated in the media containing 200 μM H_2O_2 only (first row) and in the media containing 200 μM H_2O_2 and PLGA microparticles loaded with EGCG and MnO_2 nanosheets (second row). The particle concentration was 1000 μg mL^{-1}. Blue color represents nuclei, and green color intensity represents intracellular oxidative stress level. The scale bars represent 10 μm.

nanosheet-loaded PLGA nanoparticle also showed enhanced BSA release in H_2O_2 condition, while the release rate of nanoparticle was faster than that of microparticle (Figure S8).

We further examined whether the release rate of BSA is related to the hydraulic pressure difference between the interior and exterior of the PLGA microparticles increased by the O_2 generation. The total flux of BSA (J_s) across the PLGA layer was attributed to both diffusion by the osmotic pressure difference and convection by the increased water flux (J_v), which was estimated by the Kedem-Katchalsky equations as shown below:[30−33]

$$J_s = \omega\Delta\Pi + (1-\sigma)\bar{c}J_v \quad (1)$$

$$J_v = L_p(\Delta P - \sigma\Delta\Pi) \quad (2)$$

Where L_p, ω, and σ are the transport coefficients of filtration, solute permeability, and reflection coefficient of PLGA particles, respectively; $\Delta\Pi = RT\Delta c$ is the osmotic pressure difference with R as the gas constant, T the temperature, and Δc the concentration difference of BSA between inside and outside the particles; $\bar{c}$ is the average concentration of BSA across the PLGA microparticle; $\Delta P = P_1 - P_2$ is the hydraulic pressure difference with P_1 as the internal pressure of particle and P_2 the external pressure of particle. The equation for the calculation of the rate of BSA diffusion transport (J_s) could be rewritten by combining eq 1 with eq 2 as below:

$$J_s = a\Delta c + b\Delta P \quad (3)$$

where $a = RT[\omega - \sigma(1-\sigma)\bar{c}L_p]$ and $b = (1-\sigma)\bar{c}L_p$ are the constant values, and Δc is the concentration difference of BSA between particle interior and exterior. As such, J_s is attributed to Δc and ΔP. Δc can be approximated to be constant and equal to the concentration of BSA inside the PLGA particle because the concentration of BSA in the particle interior is several orders of magnitude higher than that in the particle exterior. Therefore, in the presence of H_2O_2, J_s becomes primarily dependent on the ΔP. We calculated the ΔP values of particles subject to the different concentrations of H_2O_2 (details are described in the Supporting Information). As shown in Figure 3C, the release rate of BSA molecules was linearly related to the calculated ΔP. In accordance with the results, the release rate of BSA was significantly controlled by the internal pressure change of particles.

3.4. Active Antioxidizing Protection for Endothelial Cells and Brain Tissues from Oxidative Damage. The H_2O_2-responsive active release system was examined with EGCG, the promising polyphenolic antioxidant extracted from green tea.[16,34−37] EGCG molecules were simultaneously encapsulated in PLGA particles with and without MnO_2 nanosheets. The release rates of EGCG were measured by incubating particles in PBS containing 200 μM H_2O_2. Similar to the results observed in the BSA release, the release rate of

DOI: 10.1021/acsami.7b12297
ACS Appl. Mater. Interfaces 2017, 9, 35642−35650

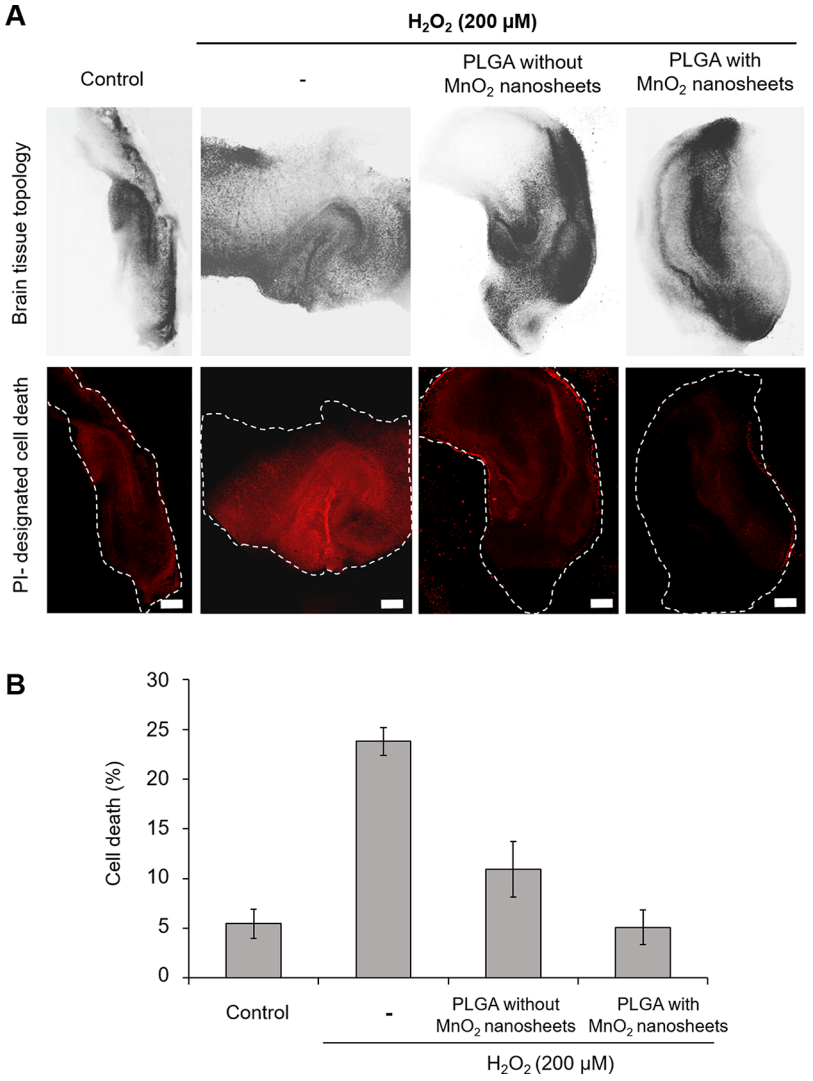

Figure 5. Activity of PLGA microparticles to protect hippocampal brain tissue explants from oxidative damage. (A) Confocal images depicting the necrotic area in brain slices after incubation in the media with four different conditions: control (0 μM H_2O_2), 200 μM H_2O_2 only, and 200 μM H_2O_2 mixed with EGCG-encapsulated PLGA microparticles without and with MnO_2 nanosheets. The images on the first-row display cross-section of the brain slice. The red color in the second-row images represents the necrotic region marked by the propidium iodide (PI) incorporation. Dotted lines in the second-row highlight the boundary of brain tissue. The scale bars represent 500 μm. (B) Quantification of the percentage of necrotic cells in brain tissues incubated in various conditions.

EGCG from the PLGA microparticles with MnO_2 nanosheets highly increased compared to that of the particle without MnO_2 nanosheets (Figure 4A).

Then, the antioxidative activity of particles was tested with endothelial cells exposed to 200 μM H_2O_2. In accordance with the MTT assay, which quantifies the fraction of metabolically active cells, 40% of the cells lost their metabolic activity when they were exposed to H_2O_2 (Figure 4B). PLGA microparticles encapsulated with EGCG but without MnO_2 nanosheets did not increase the metabolic activity. In contrast, the PLGA microparticles encapsulated with EGCG and MnO_2 nanosheets significantly increased the fraction of metabolically active cells up to 80% when increasing the particle concentration to 1.0 mg mL^{-1}. The capability of PLGA particles to protect endothelial cells from the H_2O_2-induced oxidative damage became more significant as the concentration of H_2O_2 in media increased to 400 μM (Figure 4C). In particular, the fraction of metabolically active cells incubated including the PLGA particles with MnO_2 nanosheets was 2-fold higher than that of the PLGA particles without MnO_2 nanosheets.

The intracellular oxidative stress level was also examined using CellROX Green fluorogenic probe that binds to nucleic and mitochondrial DNA and generates high fluorescence by oxidation. Cells exposed to 200 μM H_2O_2 displayed high fluorescent intensities around the nuclei (Figure 4D). In contrast, the minimal level of fluorescence was found in endothelial cells incubated with the PLGA particles containing EGCG and MnO_2 nanosheets. Therefore, it is confirmed that H_2O_2-responsive, self-pressurizing particles improve antioxidizing efficacy of EGCG by retaining metabolic activities and minimizing oxidative stress level of cells. It is likely that the cell uptake of these PLGA microparticles is minimal during the treatment.[38,39]

Furthermore, the antioxidation activity of the PLGA microparticles encapsulating EGCG and MnO_2 nanosheets was evaluated by using a brain slice explant exposed to H_2O_2. Organotypic rat brain slices were exposed to 200 μM H_2O_2 for

DOI: 10.1021/acsami.7b12297
ACS Appl. Mater. Interfaces 2017, 9, 35642−35650

inducing death of brain cells. The cellular death in brain tissues was identified by propidium iodide incorporated into membrane-compromised cells (Figure 5A). The cell death level per slice was quantified as a percentage of total cell death as measured by fluorescence from the propidium iodide. The hippocampal brain slice incubated solely with H_2O_2 showed a high intensity of red fluorescence. In accordance with the quantification made with the image, 25% of the cells within the tissue became necrotic (Figure 5B).

EGCG-loaded PLGA microparticles were incubated with brain slices to simulate the postsurgical procedure to administer anti-inflammatory drugs locally before closure. EGCG-loaded PLGA microparticles without MnO_2 nanosheets reduced the cell death level to 12%. Interestingly, PLGA microparticles encapsulating EGCG and MnO_2 nanosheets further decreased the fraction of necrotic cells to 5% that is equal to the cell death level in the control brain slice (0 μM H_2O_2). This result reaffirms that the on-demand pressurized release of EGCG can neutralize the oxidative environment in tissue more efficiently than the diffusion-based release.

4. CONCLUSION

In summary, this study demonstrates an active antioxidizing polymeric particle that can increase the internal pressure in response to the abnormal ROS level and thus actively discharge antioxidants to protect cells and tissues from oxidative damage. The active antioxidant-releasing particle was assembled by simultaneously loading MnO_2 nanosheets and green tea-derived antioxidants into PLGA particles. The MnO_2 nanosheets in the core of PLGA particle steadily decomposed H_2O_2 and generated O_2 gas that can act as a pressurizer. Accordingly, the active antioxidizing particle system could release a larger fraction of antioxidants and effectively protect endothelial cells and brain tissues from H_2O_2-induced oxidative damage. Therefore, we expect that this study would significantly impact the current design paradigm of controlled molecular releasing systems and subsequently improve the efficacy of a broad array of molecular cargos.

■ ASSOCIATED CONTENT

Supporting Information

The Supporting Information is available free of charge on the ACS Publications website at DOI: 10.1021/acsami.7b12297.

Theoretical calculation for internal pressure of polymer particles, electron microscopic images, size distribution curves for particles, zeta potential results, H_2O_2 and O_2 concentration curves, and molecular release profiles (PDF)

■ AUTHOR INFORMATION

Corresponding Author

*E-mail: hjkong06@illinois.edu.

ORCID

Jonghwi Lee: 0000-0003-2336-8695

Hyunjoon Kong: 0000-0003-4680-2968

Notes

The authors declare no competing financial interest.

■ ACKNOWLEDGMENTS

This work was supported by the National Institutes of Health (Grant 1R01 HL109192 to H.K., Grant 1U01 MH 109062 to M.U.G.), and the National Science Foundation (STC-EBICS Grant CBET-0939511 to H.K. and M.U.G., Grant DBI 14-50962 EAGER to M.U.G., and Grant CBET-1009465 to B.H.). This work was also supported by the Department of Defense Vision Research Program under Award W81XWH-17-1-022. Opinions and recommendations are those of the author and are not necessarily endorsed by the Department of Defense. J.L. and J.Y.T. acknowledge the A*STAR Graduate Scholarship (Overseas) from the Agency for Science, Technology, and Research (A*STAR). Electron microscopy was performed at the Frederick Seitz Materials Research Laboratory Central Facilities at the University of Illinois. ICP/AES was conducted at Microanalysis Laboratory (SCS CORES) at the University of Illinois. Y.S. thanks J.S. (Chemical & Biomolecular Engineering, UIUC) for the graphic assists and scientific discussions.

■ REFERENCES

(1) D'Autréaux, B.; Toledano, M. B. ROS as Signalling Molecules: Mechanisms that Generate Specificity in ROS Homeostasis. *Nat. Rev. Mol. Cell Biol.* **2007**, *8*, 813.

(2) Gough, D. R.; Cotter, T. G. Hydrogen Peroxide: a Jekyll and Hyde Signalling Molecule. *Cell Death Dis.* **2011**, *2*, e213.

(3) Tapeinos, C.; Pandit, A. Physical, Chemical, and Biological Structures based on ROS-Sensitive Moieties that are able to Respond to Oxidative Microenvironments. *Adv. Mater.* **2016**, *28*, 5553.

(4) Schieber, M.; Chandel, N. S. ROS Function in Redox Signaling and Oxidative Stress. *Curr. Biol.* **2014**, *24*, R453.

(5) Dixon, S. J.; Stockwell, B. R. The Role of Iron and Reactive Oxygen Species in Cell Death. *Nat. Chem. Biol.* **2013**, *10*, 9.

(6) Van de Bittner, G. C.; Dubikovskaya, E. A.; Bertozzi, C. R.; Chang, C. J. In vivo Imaging of Hydrogen Peroxide Production in a Murine Tumor Model with a Chemoselective Bioluminescent Reporter. *Proc. Natl. Acad. Sci. U. S. A.* **2010**, *107*, 21316.

(7) Gillette, M. U.; Wang, T. A. Brain Circadian Oscillators and Redox Regulation in Mammals. *Antioxid. Redox Signaling* **2014**, *20* (18), 2955.

(8) Yu, Z.; Sun, Q.; Pan, W.; Li, N.; Tang, B. A Near-Infrared Triggered Nanophotosensitizer Inducing Domino Effect on Mitochondrial Reactive Oxygen Species Burst for Cancer Therapy. *ACS Nano* **2015**, *9* (11), 11064.

(9) Kwon, H. J.; Cha, M.-Y.; Kim, D.; Kim, D. K.; Soh, M.; Shin, K.; Hyeon, T.; Mook-Jung, I. Mitochondria-Targeting Ceria Nanoparticles as Antioxidants for Alzheimer's Disease. *ACS Nano* **2016**, *10*, 2860.

(10) Zhang, J.; Zhen, X.; Upputuri, P. K.; Pramanik, M.; Chen, P.; Pu, K. Activatable Photoacoustic Nanoprobes for In Vivo Ratiometric Imaging of Peroxynitrite. *Adv. Mater.* **2017**, *29*, 1604764.

(11) Rains, J. L.; Jain, S. K. Oxidative Stress, Insulin Signaling, and Diabetes. *Free Radical Biol. Med.* **2011**, *50* (5), 567.

(12) Feeney, C. J.; Frantseva, M. V.; Carlen, P. L.; Pennefather, P. S.; Shulyakova, N.; Shniffer, C.; Mills, L. R. Vulnerability of Glial Cells to Hydrogen Peroxide in Cultured Hippocampal Slices. *Brain Res.* **2008**, *1198*, 1.

(13) Fan, W.; Bu, W.; Shen, B.; He, Q.; Cui, Z.; Liu, Y.; Zheng, X.; Zhao, K.; Shi, J. Intelligent MnO2 Nanosheets Anchored with Upconversion Nanoprobes for Concurrent pH-/H_2O_2-Responsive UCL Imaging and Oxygen-Elevated Synergetic Therapy. *Adv. Mater.* **2015**, *27*, 4155.

(14) Grant, S. S.; Hung, D. T. Persistent Bacterial Infections, Antibiotic Tolerance, and the Oxidative Stress Response. *Virulence* **2013**, *4* (4), 273.

(15) Pisoschi, A. M.; Pop, A. The Role of Antioxidants in the Chemistry of Oxidative Stress: A Review. *Eur. J. Med. Chem.* **2015**, *97*, 55.

(16) Chung, J. E.; Tan, S.; Gao, S. J.; Yongvongsoontorn, N.; Kim, S. H.; Lee, J. H.; Choi, H. S.; Yano, H.; Zhuo, L.; Kurisawa, M.; Ying, J. Y. Self-Assembled Micellar Nanocomplexes Comprising Green Tea

DOI: 10.1021/acsami.7b12297
ACS Appl. Mater. Interfaces 2017, 9, 35642−35650

Catechin Derivatives and Protein Drugs for Cancer Therapy. *Nat. Nanotechnol.* **2014**, *9*, 907.
(17) Hood, E.; Simone, E.; Wattamwar, P.; Dziubla, T.; Muzykantov, V. Nanocarriers for Vascular Delivery of Antioxidants. *Nanomedicine* **2011**, *6* (7), 1257.
(18) Munin, A.; Edwards-Levy, F. Encapsulation of Natural Polyphenolic Compounds; a Review. *Pharmaceutics* **2011**, *3*, 793.
(19) Granja, A.; Pinheiro, M.; Reis, S. Epigallocatechin Gallate Nanodelivery Systems for Cancer Therapy. *Nutrients* **2016**, *8*, 307.
(20) Singh, M.; Bhatnagar, P.; Mishra, S.; Kumar, P.; Shukla, Y.; Gupta, K. C. PLGA-Encapsulated Tea Polyphenols Enhance the Chemotherapeutic Efficacy of Cisplatin against Human Cancer Cells and Mice Bearing Ehrlich Ascites Carcinoma. *Int. J. Nanomed.* **2015**, *10*, 6789.
(21) Mura, S.; Nicolas, J.; Couvreur, P. Stimuli-Responsive Nanocarriers for Drug Delivery. *Nat. Mater.* **2013**, *12*, 991.
(22) Hines, D. J.; Kaplan, D. L. Poly (Lactic-co-Glycolic) Acid–Controlled-Release Systems: Experimental and Modeling Insights. *Crit. Rev. Ther. Drug Carrier Syst.* **2013**, *30*, 257.
(23) Zolnik, B. S.; Burgess, D. J. Effect of Acidic pH on PLGA Microsphere Degradation and Release. *J. Controlled Release* **2007**, *122*, 338.
(24) Zhao, Z.; Fan, H.; Zhou, G.; Bai, H.; Liang, H.; Wang, R.; Zhang, X.; Tan, W. Activatable Fluorescence/MRI Bimodal Platform for Tumor Cell Imaging via MnO_2 Nanosheet–Aptamer Nanoprobe. *J. Am. Chem. Soc.* **2014**, *136*, 11220.
(25) Chen, Y.; Ye, D.; Wu, M.; Chen, H.; Zhang, L.; Shi, J.; Wang, L. Break-up of Two-Dimensional MnO_2 Nanosheets Promotes Ultrasensitive pH-Triggered Theranostics of Cancer. *Adv. Mater.* **2014**, *26*, 7019.
(26) Halliwell, B.; Clement, M. V.; Long, L. H. Hydrogen Peroxide in the Human Body. *FEBS Lett.* **2000**, *486*, 10.
(27) Sah, H.; Toddywala, R.; Chien, Y. W. The Influence of Biodegradable Microcapsule Formulations on the Controlled Release of a Protein. *J. Controlled Release* **1994**, *30*, 201.
(28) Yeo, Y.; Park, K. Control of Encapsulation Efficiency and Initial Burst in Polymeric Microparticle Systems. *Arch. Pharmacal Res.* **2004**, *27*, 1.
(29) Li, Y.-P.; Pei, Y.-Y.; Zhang, X.-Y.; Gu, Z.-H.; Zhou, Z.-H.; Yuan, W.-F.; Zhou, J.-J.; Zhu, J.-H.; Gao, X.-J. PEGylated PLGA Nanoparticles as Protein Carriers: Synthesis, Preparation and Biodistribution in Rats. *J. Controlled Release* **2001**, *71*, 203.
(30) Jarzyńska, M.; Pietruszka, M. The Application of the Kedem–Katchalsky Equations to Membrane Transport of Ethyl Alcohol and Glucose. *Desalination* **2011**, *280*, 14.
(31) Suchanek, G. Mechanistic Equations for Membrane Transport of Multicomponent Solutions. *Gen. Physiol. Biophys.* **2006**, *25*, 53.
(32) Truskey, G. A.; Yuan, F.; Katz, D. F. Transport Phenomena in Biological Systems. *Transport Phenomena in Biological Systems*, 2nd ed.; Pearson Prentice Hall: Upper Saddle River, NJ, 2009; pp 447–449.
(33) Ozcelikkale, A.; Moon, H.; Linnes, M.; Han, B. In Vitro Microfluidic Models of Tumor Microenvironment to Screen Transport of Drugs and Nanoparticles. *WIREs Nanomed. Nanobiotechnol.* **2017**, *9*, e1460.
(34) Zaveri, N. T. Green Tea and Its Polyphenolic Catechins: Medicinal Uses in Cancer and Noncancer Applications. *Life Sci.* **2006**, *78*, 2073.
(35) Yagi, H.; Tan, J.; Tuan, R. S. Polyphenols Suppress Hydrogen Peroxide-Induced Oxidative Stress in Human Bone-Marrow Derived Mesenchymal Stem Cells. *J. Cell. Biochem.* **2013**, *114* (5), 11163.
(36) Singh, B. N.; Shankar, S.; Srivastava, R. K. Green Tea Catechin, Epigallocatechin-3-Gallate (EGCG): Mechanisms, Perspectives and Clinical Applications. *Biochem. Pharmacol.* **2011**, *82*, 1807.
(37) Afzal, M.; Safer, A. M.; Menon, M. Green Tea Polyphenols and Their Potential Role in Health and Disease. *Inflammopharmacology* **2015**, *23*, 151.
(38) Blanco, E.; Shen, H.; Ferrari, M. Principles of nanoparticle design for overcoming biological barriers to drug delivery. *Nat. Biotechnol.* **2015**, *33*, 941.
(39) Xu, A.; Yao, M.; Xu, G.; Ying, J.; Ma, W.; Li, B.; Jin, Y. A physical model for the size-dependent cellular uptake of nanoparticles modified with cationic surfactants. *Int. J. Nanomed.* **2012**, *7*, 3547.

DOI: 10.1021/acsami.7b12297
ACS Appl. Mater. Interfaces 2017, 9, 35642–35650